A Graph Auto-Encoder for Haplotype Assembly and Viral Quasispecies Reconstruction

Ziqi Ke and Haris Vikalo
Department of Electrical and Computer Engineering
The University of Texas at Austin
ziqike@utexas.edu, hvikalo@ece.utexas.edu

Abstract

Reconstructing components of a genomic mixture from data obtained by means of DNA sequencing is a challenging problem encountered in a variety of applications including single individual haplotyping and studies of viral communities. High-throughput DNA sequencing platforms oversample mixture components to provide massive amounts of reads whose relative positions can be determined by mapping the reads to a known reference genome; assembly of the components, however, requires discovery of the reads' origin – an NP-hard problem that the existing methods struggle to solve with the required level of accuracy. In this paper, we present a learning framework based on a graph auto-encoder designed to exploit structural properties of sequencing data. The algorithm is a neural network which essentially trains to ignore sequencing errors and infers the posterior probabilities of the origin of sequencing reads. Mixture components are then reconstructed by finding consensus of the reads determined to originate from the same genomic component. Results on realistic synthetic as well as experimental data demonstrate that the proposed framework reliably assembles haplotypes and reconstructs viral communities, often significantly outperforming state-of-the-art techniques.

1 Introduction

Genetic makeup of a biological sample, inferred by means of DNA sequencing, will help determine an individual's susceptibility to a broad range of chronic and acute diseases, support the discovery of new pharmaceutical products, and personalize and improve the delivery of health care. However, before the promises of personalized medicine come to fruition, efficient methods for accurate inference of genetic variations from massive DNA sequencing data must be devised.

Information about variations in an individual genome is provided by haplotypes, ordered lists of single nucleotide polymorphisms (SNPs) on the individual's chromosomes (Schwartz 2010). High-throughput DNA sequencing technologies generate massive amounts of reads that sample an individual genome and thus enable studies of genetic variations (Schwartz 2010; Clark 2004; Sabeti 2002). Haplotype reconstruction, however, remains challenging due to limited lengths of reads and presence of sequencing errors (Hashemi 2018). Particularly difficult is the assembly of haplotypes in polyploids, organisms with chromosomes organized in k-tuples with $k > 2$, where deep coverage is typically required to achieve desired accuracy. This implies high cost and often renders existing haplotype assembly techniques practically infeasible (Motazedi 2018).

A closely related problem to haplotype assembly is that of reconstructing viral communities. RNA viruses such as hepatitis, HIV, and Ebola, are characterized by high mutation rates which give rise to communities of viral genomes, the so-called viral quasispecies. Determining genetic diversity of a virus is essential for the understanding of its origin and mutation patterns, and the development of effective drug treatments. Reconstructing viral quasispecies (i.e., *viral haplotypes*, as we refer to them for convenience) is even more challenging than haplotype assembly (Ahn 2018) since the number of constituent strains in a community is typically unknown, and its spectra (i.e., strain frequencies) non-uniform.

Existing methods often approach haplotype assembly as the task of grouping sequencing reads according to their chromosomal origin into as many clusters as there are chromosomes. Separation of reads into clusters is rendered challenging by their limited lengths and the presence of sequencing errors (Hashemi 2018); such artifacts create ambiguities regarding the origin of the reads. The vast majority of existing haplotype assembly methods attempt to remove the aforementioned ambiguity by altering or even discarding the data, leading to minimum SNP removal (Lancia 2001), maximum fragments cut (Duitama 2010), and minimum error correction (MEC) score (Lippert 2002) optimization criteria. Majority of haplotype assembly methods developed in recent years are focused on optimizing the MEC score, i.e., determining the smallest possible number of nucleotides in sequencing reads that should be altered such that the resulting dataset is consistent with having originated from k haplotypes (k denotes the ploidy of an organism) (Xie 2016; Pirola 2015; Kuleshov 2014; Patterson 2015; Bonizzoni 2016). These include the branch-and-bound scheme (Wang 2005), an integer linear programming formulation in (Chen 2013), and a dynamic programming framework in (Kuleshov 2014). All these tech-

*This work was funded in part by the NSF grant CCF 1618427.

niques attempt to find exact solution to the MEC score minimization problem; the resulting high complexity has motivated search for computationally efficient heuristics. They include the greedy algorithm in (Levy 2007) and methods that compute posterior joint probability of the alleles in a haplotype sequence via MCMC (Bansal 2008) and Gibbs (Kim 2007) sampling. A max-cut algorithm for haplotype assembly in (Bansal 2008) is motivated by the clustering interpretation of the problem. The efficient algorithm proposed there, HapCUT, has recently been upgraded as HapCUT2 (Edge 2017). In (Aguiar 2012), a novel flow-graph approach to haplotype assembly was proposed, demonstrating performance superior to state-of-the-art methods. More recent methods include a greedy max-cut approach in (Duitama 2011), convex optimization framework in (Das 2015), and a communication-theoretic motivated algorithm in (Puljiz 2016).

Haplotype assembly for polyploids ($k > 2$) is more challenging than that for diploids ($k = 2$) due to a much larger space of possible solutions to be searched. Among the aforementioned methods, only HapCompass (Aguiar 2012), SDhaP (Das 2015) and BP (Puljiz 2016) are capable of solving the haplotype assembly problem for $k > 2$. Other techniques that can handle reconstruction of haplotypes for both diploid and polyploid genomes include a Bayesian method HapTree (Berger 2014), a dynamic programming method H-PoP (Xie 2016) shown to be more accurate than the techniques in (Aguiar 2012; Berger 2014; Das 2015), and the matrix factorization schemes in (Cai 2016; Hashemi 2018).

On another note, a number of viral quasispecies reconstruction methods were proposed in recent years. Examples include ShoRAH (Zagordi 2011) and ViSpA (Astrovskaya 2011) that perform read clustering and read-graph path search, respectively, to identify distinct viral components. QuasiRecomb (Töpfer 2013) casts the problem as the decoding in a hidden Markov model while QuRe (Prosperi 2012) formulates it as a combinatorial optimization. PredictHaplo (Prabhakaran 2014) employs non-parametric Bayesian techniques to automatically discover the number of viral strains in a quasispecies. More recently, aBayesQR (Ahn 2017) approached viral quasispecies reconstruction with a combination of hierarchical clustering and Bayesian inference while (Ahn 2018) relies on tensor factorization.

In this paper, we propose a first ever neural network-based learning framework, named GAEseq, to both haplotype assembly and viral quasispecies reconstruction problems. The framework aims to estimate the posterior probabilities of the origins of sequencing reads using an auto-encoder whose design incorporates salient characteristics of the sequencing data. Auto-encoders (Fukushima 1975) are neural networks that in an unsupervised manner learn a low-dimensional representation of data; more specifically, they attempt to perform a dimensionality reduction while robustly capturing essential content of high-dimensional data (Goodfellow 2016). Auto-encoders have shown outstanding performance in a variety of applications across different fields including natural language processing (Socher 2011), collaborative filtering (Rianne 2017), and information retrieval (Thomas 2016), to name a few. Typically, auto-encoders consist of two blocks: an encoder and a decoder. The encoder converts input data into the so-called codes while the decoder reconstructs the input from the codes. The act of copying the input data to the output would be of little interest without an important additional constraint – namely, the constraint that the dimension of codes is smaller than the dimension of the input. This enables auto-encoders to extract salient features of the input data. For both the single individual and viral haplotype reconstruction problems, the salient features of data are the origins of sequencing reads. In our work, we propose a graph auto-encoder architecture with an encoder featuring a softmax function placed after the dense layer that follows graph convolutional layers (Masci 2011; Rianne 2017); the softmax function acts as an estimator of the posterior probabilities of the origins of sequencing reads. The decoder assembles haplotypes by finding the consensus sequence for each component of the mixture, thus enabling end-to-end solution to the reconstruction problems.

2 Methods

2.1 Problem formulation

Let H denote a $k \times n$ haplotype matrix where k is the number of (single individual or viral) haplotypes and n is the haplotype length. Furthermore, let R denote an $m \times n$ SNP fragment matrix whose rows correspond to sequencing reads and columns correspond to SNP positions. Matrix R is formed by first aligning reads to a reference genome and then identifying and retaining only the information that the reads provide about heterozygous genomic sites. One can interpret R as being obtained by sparsely sampling an underlying ground truth matrix M, where the i^{th} row of M is the haplotype sampled by the i^{th} read. The sampling is sparse because the reads are much shorter than the haplotypes; moreover, the reads may be erroneous due to sequencing errors. Following (Ahn 2018) , we formalize the sampling operation as

$$[\mathcal{P}_\Omega(M)]_{ij} = \begin{cases} M_{ij}, & (i,j) \in \Omega \\ 0, & \text{otherwise} \end{cases} \tag{1}$$

where Ω denotes the set of informative entries in R, i.e., the set of (i,j) such that the j^{th} SNP is covered by the i^{th} read, and $\mathcal{P}_\Omega$ is the projection operator denoting the sampling of haplotypes by reads. Sequencing is erroneous and thus $[\mathcal{P}_\Omega(R)]_{ij}$ may differ from $[\mathcal{P}_\Omega(M)]_{ij}$; in particular, given sequencing error rate p, $[\mathcal{P}_\Omega(R)]_{ij} = [\mathcal{P}_\Omega(M)]_{ij}$ with probability $1-p$.

Since each read samples one of the haplotypes, $R = \mathcal{P}_\Omega(UH)$ where U denotes the $m \times k$ matrix indicating origins of the reads in R. In particular, each row of matrix U is one of the k-dimensional standard unit vectors $e_i^{(k)}, 1 \leq i \leq k$, with 1 in the i^{th} position and the remaining entries 0. If i^{th} read samples j^{th} haplotype, the i^{th} row of U is $e_j^{(k)}$. If the origins of reads were known, each haplotype could be reconstructed by finding consensus of reads which sample that particular haplotype. We think of the assembly as a two-step procedure: given the SNP fragment matrix R we first identify the read origin indicator matrix U and then use U to reconstruct the haplotype matrix H.

To characterize the performance of haplotype assembly methods we rely on two metrics: the minimum error correction (MEC) score, which can be traced back to (Lippert 2002), and the correct phasing rate, also referred to as reconstruction rate. The MEC score is defined as the smallest number of observed entries in R that need to be altered (i.e., corrected) such that the resulting data is consistent with having originated from k distinct haplotypes, i.e.,

$$\text{MEC} = \sum_{i=1}^{m} \min_{j=1,2,\dots,k} \text{HD}(R_{i:}, H_{j:}), \qquad (2)$$

where $\text{HD}(\cdot,\cdot)$ denotes the Hamming distance between its arguments (sequences, evaluated only over informative entries), $R_{i:}$ denotes the i^{th} row of R and $H_{j:}$ denotes the j^{th} row of H. The correct phasing rate (CPR) is defined as

$$\text{CPR} = 1 - \frac{1}{kn}(\min \sum_{i=1}^{k} \text{HD}(H_{i:}, \mathcal{M}(H_{i:}))), \qquad (3)$$

where $\mathcal{M}$ is the one-to-one mapping from the set of reconstructed haplotype to the set of true haplotype (Hashemi 2018), i.e., mapping that determines the best possible match between the two sets of haplotypes. To characterize performance of methods for reconstruction of viral quasispecies with generally a priori unknown number of components, in addition to correct phasing rate we also quantify *recall rate*, defined as the fraction of perfectly reconstructed components in a population (i.e., recall rate = $\frac{TP}{TP+FN}$), and *predicted proportion*, defined as the ratio of the estimated and the true number of components in a genomic mixture (Ahn 2018).

To assemble haplotypes from a set of reads we design and employ a graph auto-encoder. Fig. 1 (b) shows the entire end-to-end pipeline that takes the collection of erroneous reads and generates reconstructed haplotypes. First, the SNP fragment matrix R is processed by the graph encoder to infer the read origin indicator matrix U; then, a haplotype decoder reconstructs matrix H. The graph auto-encoder is formalized in the next section.

2.2 Graph auto-encoders

Graph auto-encoders are a family of auto-encoders specifically designed for learning on graph-structured data (Rianne 2017; Thomas 2016). In this paper, we design graph auto-encoders for the assembly of the components of a genomic mixture. As in conventional auto-encoder structures, the developed architecture consists of two parts: the graph encoder and the decoder. The graph encoder $Z = f(R, A)$ takes the SNP fragment matrix R and the $m \times n$ graph adjacency matrix A as inputs, and outputs the $m \times k$ node embedding matrix Z. Note that we impose constraints on the node embedding matrix so that the salient features extracted by a graph auto-encoder approximate the read origin indicator matrix U. Such a constraint does not prevent efficient training of the auto-encoders via backpropagation. The decoder $\hat{R} = g(Z)$ is utilized to reconstruct the SNP fragment matrix R and the haplotype matrix H from the node embedding matrix Z; this implies that the decoder is essentially capable of imputing the unobserved entries in the SNP fragment matrix.

To numerically represent information in the SNP fragment matrix R, we encode its entries R_{ij} using a set of 4 discrete values – one for each of 4 possible nucleotides – where the mapping between nucleotides and the discrete values can be decided arbitrarily. To this end, we may simply represent the nucleotides A, C, G and T by 1, 2, 3 and 4, respectively; non-informative entries in each row of R, i.e., SNP positions not covered by a read, are represented by 0. Note that the SNP fragment matrix can be represented by an undirected bipartite graph $G = (V, E, \mathcal{W})$ where the set of read nodes $r_i \in \mathcal{A}$ with $i \in \{1, ..., m\}$ and the set of SNP nodes $s_j \in \mathcal{B}$ with $j \in \{1, ..., n\}$ together form the set of vertices V, i.e., $\mathcal{A} \cup \mathcal{B} = V$. The weights $w \in \{1, 2, 3, 4\} = \mathcal{W}$ assigned to edges $(r_i, w, s_j) \in E$ are the discrete values used to represent nucleotides. With this model in place, we can rephrase the graph encoder as $Z = f(R, A_1, A_2, A_3, A_4)$, where $A_w \in \{0, 1\}^{m \times n}$ represents the graph adjacency matrix for a nucleotide encoded by w. Equivalently, A_w has 1's for the entries whose corresponding positions in R are encoded by w. Since we are interested in imputing the unobserved entries based on the observed entries in R instead of simply copying the observed entries to $\hat{R}$, it is beneficial to reformulate the decoder as $\hat{R} = g(Z, R)$. In other words, the auto-encoder is trained to learn from the observed entries in order to determine origin of reads, impute unobserved entries of R, and reconstruct haplotypes in the genomic mixture.

2.3 Read origin detection via graph encoder

Recall the interpretation that the SNP fragment matrix R is obtained by erroneously sampling an underlying ground truth matrix M. This motivates development of a specific graph encoder architecture, motivated by the ideas of the design in (Rianne 2017), that is capable of detecting origin of sequencing reads in R via estimating the posterior probabilities of the origin of each read.

Let D_r denote an $m \times m$ diagonal read degree matrix whose entries indicate the number of SNPs covered by each read, and let D_s denote an $n \times n$ diagonal SNP degree matrix whose entries indicate the number of reads covering each SNP. We facilitate exchange of messages between read nodes and SNP nodes in the graph, initiating it from the set of read nodes $\mathcal{A}$; doing so helps reduce the dimensions of weights and biases since the number of reads m is far greater than the haplotype length n. Note that the dimension of messages keeps reducing during the message passing procedure.

The messages from read nodes to SNP nodes are defined as

$$M_{(1)} = \sigma(\sum_{w=1}^{4} D_s^{-1} A_w^T R W_w^{(1)} + B_w^{(1)}), \qquad (4)$$

where $W_w^{(1)}$ and $B_w^{(1)}$ denote the weights and biases of the first convolutional layer for the nucleotide encoded with w, respectively, σ denotes an element-wise activation function such as $\text{ReLU}(\cdot) = \max(\cdot, 0)$, and $(\cdot)^T$ denotes the transpose of a matrix. The dimension of both $W_w^{(1)}$ and $B_w^{(1)}$ is $n \times c_{(1)}$, where $c_{(1)}$ denotes the message length after the first message passing step.

The messages from SNP nodes to read nodes are defined

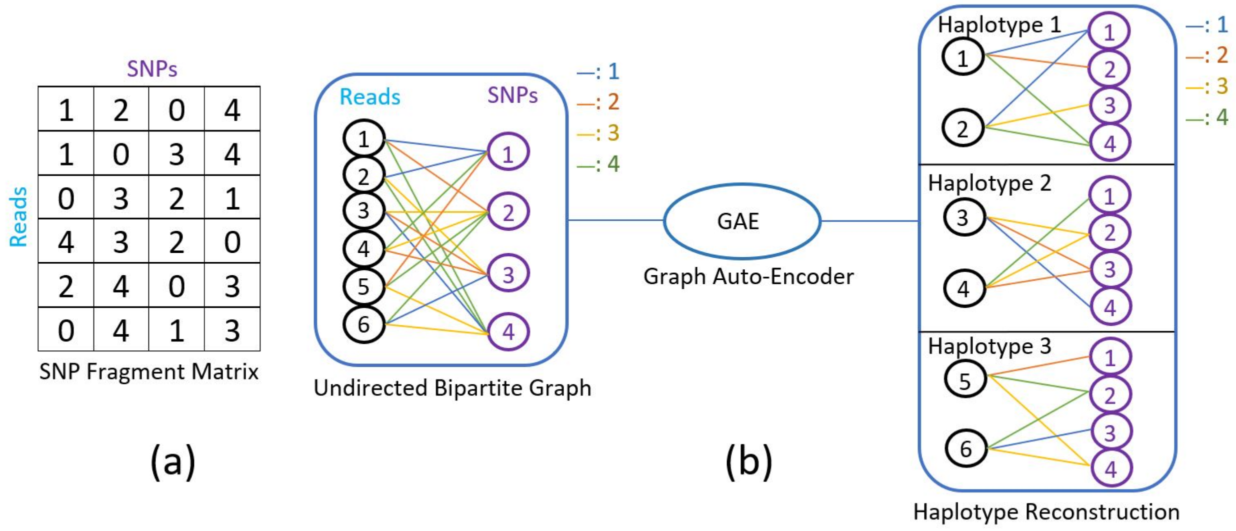

1	2	0	4
1	0	3	4
0	3	2	1
4	3	2	0
2	4	0	3
0	4	1	3

Figure 1: (a) Segment of the SNP fragment matrix. Non-zero entries represent SNP information provided by sequencing reads; labels 1-4 indicate the four nucleotides. Zero entries in a row indicate that the read does not cover corresponding SNP. In this illustration, the first two rows represent reads originating from the same haplotype; the third and fourth reads both originated from another haplotype; and so on. (b) The pipeline from the SNP fragment matrix to haplotypes via a graph auto-encoder.

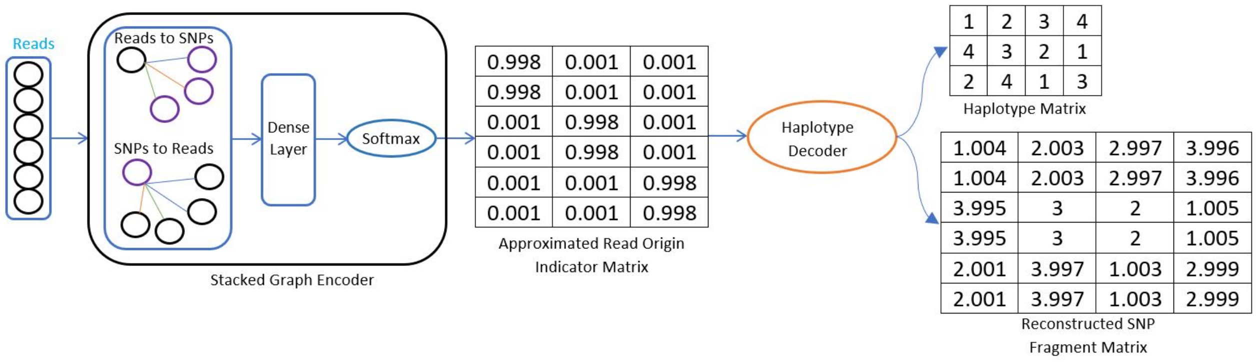

0.998	0.001	0.001
0.998	0.001	0.001
0.001	0.998	0.001
0.001	0.998	0.001
0.001	0.001	0.998
0.001	0.001	0.998

1	2	3	4
4	3	2	1
2	4	1	3

1.004	2.003	2.997	3.996
1.004	2.003	2.997	3.996
3.995	3	2	1.005
3.995	3	2	1.005
2.001	3.997	1.003	2.999
2.001	3.997	1.003	2.999

Figure 2: A forward pass through the graph auto-encoder consisting of a stacked graph encoder that passes messages between read and SNP nodes and constructs approximate read origin indicator matrix via the softmax function. Decoder reconstructs haplotypes and SNP fragment matrix.

as

$$M_{(2)} = \sigma(\sum_{w=1}^{4} D_r^{-1} A_w M_{(1)} W_w^{(2)} + B_w^{(2)}), \quad (5)$$

where $W_w^{(2)}$ and $B_w^{(2)}$ denote the weights and biases of the second convolutional layer for the nucleotide encoded with w, respectively. The dimension of both $W_w^{(2)}$ and $B_w^{(2)}$ is $c_{(1)} \times c_{(2)}$, where $c_{(2)}$ denotes the message length after the second message passing step.

Repeating message passing and stacking the convolutional layers leads to formation of a deep model. The read nodes to SNP nodes layer is readily generalized as

$$M_{(2i+1)} = \sigma(\sum_{w=1}^{4} D_s^{-1} A_w^T M_{(2i)} W_w^{(2i+1)} + B_w^{(2i+1)}), \quad (6)$$

where $i \in \{0, 1, 2, ...\}$ and $M_{(2i)} = R$ for $i = 0$. The dimension of $M_{(2i)}$ is $m \times c_{(2i)}$. Furthermore, the SNP nodes to read nodes layer is generalized as

$$M_{(2i)} = \sigma(\sum_{w=1}^{4} D_r^{-1} A_w M_{(2i-1)} W_w^{(2i)} + B_w^{(2i)}), \quad (7)$$

where $i \geq 1$. The dimension of $M_{(2i-1)}$ is $n \times c_{(2i-1)}$. Note that the messages are passed from read nodes to SNP nodes when the subscript of M is odd, and otherwise traverse in the opposite direction.

Equation (6) and (7) specify the graph convolutional layer while the dense layer is defined as

$$O = \sigma(M_{(l)} W_d + B_d), \quad (8)$$

where O denotes the output of the dense layer, W_d and B_d are the weights and biases of the dense layer, respectively, $M_{(l)}$ is the output of the last graph convolutional layer, and l represents the number of graph convolutional layers. The dimension of W_d is $c_{(l)} \times k$ and the dimension of O and B_d is $m \times k$, where k denotes the ploidy (i.e., the number of components in a genomic mixture).

To find Z which approximates the read origin indicator matrix U (i.e., Z with each row close in the l_2-norm sense to a k-dimensional standard basis vector), we employ the softmax function

$$Z_{ij} = \frac{e^{\beta O_{ij}}}{\sum_{j=1}^{k} e^{\beta O_{ij}}}, \tag{9}$$

where in our experiments we set β to 200. Having estimated read origins by the node embedding matrix Z, the reads can be organized into k clusters. This enables straightforward reconstruction of haplotypes by determining the consensus sequence for each cluster.

2.4 Haplotype decoder

Thus far, we have conveniently been representing alleles as the numbers in $\{1, 2, 3, 4\}$. It is desirable, however, that in the definition of a loss function the distance between numerical values representing any two alleles is identical, no matter which pair of alleles is considered; this ensures the loss function relates to the MEC score – the metric of interest in haplotype assembly problems. Following (Ahn 2018), we define the loss function of the auto-encoder as the squared Frobenius norm of the difference between a one-hot SNP fragment matrix $\mathcal{R}$ and the reconstructed matrix $\hat{\mathcal{R}} = Z\mathcal{H}$ at the informative positions, i.e., $\mathcal{L} = \frac{1}{2}||\mathcal{P}_\Omega(\mathcal{R} - Z\mathcal{H})||_F^2$, where $\mathcal{R} \in \{0, 1\}^{m\times 4n}$ and $\mathcal{H} \in \{0, 1\}^{k\times 4n}$ are formed by substituting discrete values $w \in \{1, 2, 3, 4\}$ by the set of four dimensional standard basis vectors $e_i^{(4)}, 1 \leq i \leq 4$. With such a notational convention, the proposed loss function approximates the MEC score; it only approximates the score, rather than coincides with it, because Z is an approximation of the read-origin matrix U. Therefore, the graph auto-encoder is trained to approximately minimize the MEC score. Fig. 2 illustrates the data processing pipeline that takes as inputs reads in the SNP fragment matrix and produces the matrix of haplotypes as well as imputes missing entries in the SNP fragment matrix. The proposed graph auto-encoders for haplotype assembly and viral quasispecies reconstruction are formalized as Algorithm 1 and Algorithm 2, respectively. For the viral quasispecies reconstruction problem, the number of clusters k is typically unknown; detailed strategy based on (Ahn 2018) for the automated inference of k can be found in Supplementary Document B.

Algorithm 1 Graph auto-encoder for haplotype assembly

```
 1: Input: SNP fragment matrix $R$, the number of experiments $n_{exp}$ and the number of haplotpyes $k$
 2: Output: Reconstructed haplotypes $H$
 3: while $n_{exp} \neq 0$ do
 4:     Initialize $W_w^{(i)}$, $B_w^{(i)}$, $W_d$ and $B_d$ using Xavier initialization where $w \in \{1,2,3,4\}$ and $i \in \{1,2\}$
 5:     for $n_{epoch} = 1$ to 100 do
 6:         $M_{(1)} \leftarrow \sigma(\sum_w D_s^{-1} A_w^T R W_w^{(1)} + B_w^{(1)})$
 7:         $M_{(2)} \leftarrow \sigma(\sum_w D_r^{-1} A_w M_{(1)} W_w^{(2)} + B_w^{(2)})$
 8:         $O \leftarrow \sigma(M_{(2)} W_d + B_d)$
 9:         $Z_{ij} \leftarrow \frac{e^{\beta O_{ij}}}{\sum_{j=1}^{k} e^{\beta O_{ij}}}$ with $\beta = 200$
10:         Calculate $\mathcal{H}$ by majority voting
11:         $\mathcal{L} \leftarrow \frac{1}{2}||\mathcal{P}_\Omega(\mathcal{R} - Z\mathcal{H})||_F^2$
12:         Record reconstructed haplotypes and the MEC score
13:         Update $W_w^{(i)}$, $B_w^{(i)}$, $W_d$ and $B_d$ using Adam Optimizer where $w \in \{1,2,3,4\}$ and $i \in \{1,2\}$
14:     end for
15:     $n_{exp} \leftarrow n_{exp} - 1$
16: end while
17: Output the reconstructed haplotypes $H$ corresponding to the lowest MEC score
```

Algorithm 2 Graph auto-encoder for viral quasispecies reconstruction

```
 1: Input: SNP fragment matrix $R$, the number of experiments $n_{exp}$, the MEC improvement rate threshold $\eta$ and the estimated initial number of components $k_0$
 2: Output: Reconstructed viral haplotypes $H$ and the inferred frequencies
 3: Initial $\tau \leftarrow 0$, MECflag $\leftarrow 0$ and $k_\tau \leftarrow k_0$
 4: while $\tau = 0$ or $k_\tau = k_\tau - 1$ do
 5:     for $k \in \{k_\tau, k_\tau + 1\}$ do
 6:         Run Algorithm 1 with $k$
 7:     end for
 8:     if MECimpr$(k_\tau) \leq \eta$ then
 9:         $k_{\tau+1} \leftarrow \lfloor (k_\tau + \max\{1, k_i\})/2 \rfloor, \{i \in \{1, \cdots, \tau\text{-}1\} : k_i \leq k_\tau\}$; MECflag $\leftarrow 1$
10:     else
11:         if MECflag $= 0$ then
12:             $k_{\tau+1} \leftarrow 2k_\tau$
13:         else
14:             $k_{\tau+1} \leftarrow \lfloor (k_\tau + \min k_i)/2 \rfloor, \{i \in \{1, \cdots, \tau\text{-}1\} : k_i > k_\tau\}$
15:         end if
16:     end if
17:     $\tau \leftarrow \tau + 1$
18: end while
19: Output the viral quasispecies $H$ with $k = k_\tau + 1$ and the inferred frequencies
```

3 Results

The hyper-parameters of GAEseq are determined by training on 5 synthetic triploid datasets with coverage 30$\times$ and validated on different 5 synthetic triploid datasets with the same coverage. The results reported in this section are obtained on test data. Detailed description of the computational platform and the choice of hyper-parameters can be found in Supplementary Document A.

Table 1: Performance comparison on biallelic Solanum Tuberosum semi-experimental data.

Coverage		MEC		CPR	
		Mean	SD	Mean	SD
15	GAEseq	**8.200**	**4.686**	**0.822**	0.048
	HapCompass	100.700	66.150	0.763	**0.046**
	H-PoP	28.700	32.667	0.783	0.066
	AltHap	59.100	28.125	0.709	0.054
25	GAEseq	**8.400**	**4.719**	**0.831**	0.081
	HapCompass	124.800	132.156	0.810	0.063
	H-PoP	33.800	47.434	0.798	**0.046**
	AltHap	92.600	83.649	0.756	0.068
35	GAEseq	**10.700**	**3.234**	**0.857**	0.087
	HapCompass	217.400	174.135	0.775	**0.072**
	H-PoP	41.700	53.971	0.823	0.094
	AltHap	164.000	101.583	0.754	0.093

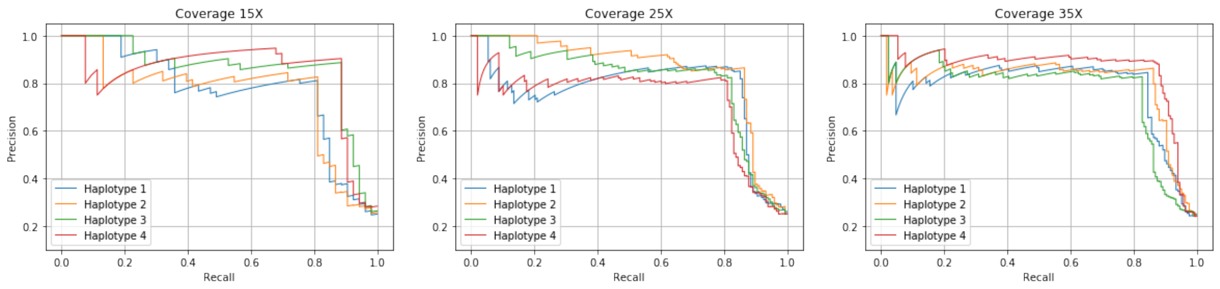

Figure 3: The precision-recall curves for Solanum Tuberosum semi-experimental data with coverage 15×, 25× and 35×

Table 2: Performance comparison of GAEseq, PredictHap, TenSQR and aBayesQR on a real HIV-1 5-virus-mix data. Genes where all the strains are perfectly reconstructed are denoted as boldface.

		p17	p24	p2-p6	PR	RT	RNase	int	vif	vpr	vpu	gp120	gp41	nef
GAEseq	PredProp	**1**	1	**1**	**1**	**1.2**	**1**	**1**	**1**	**1**	1.2	1	1	1
	CPR$_{HXB2}$	**100**	99.4	**100**	**100**	**100**	**100**	**100**	**100**	**100**	100	96.2	96.7	100
	CPR$_{89.6}$	**100**	99.4	**100**	**100**	**100**	**100**	**100**	**100**	**100**	99.2	99.4	100	98.2
	CPR$_{JR-SCF}$	**100**	100	**100**	**100**	**100**	**100**	**100**	**100**	**100**	100	99.9	100	99.3
	CPR$_{NL4-3}$	**100**	100	**100**	**100**	**100**	**100**	**100**	**100**	**100**	100	100	100	99.8
	CPR$_{YU2}$	**100**	100	**100**	**100**	**100**	**100**	**100**	**100**	**100**	100	99.6	100	98.1
PredictHap	PredProp	**1**	0.6	**1**	**1**	**1**	0.8	0.8	0.8	**1**	0.8	0.8	0.8	0.8
	CPR$_{HXB2}$	**100**	0	**100**	**100**	**100**	98.9	100	100	**100**	93.2	0	0	0
	CPR$_{89.6}$	**100**	100	**100**	**100**	**100**	100	99.8	100	**100**	0	97.8	100	98.8
	CPR$_{JR-SCF}$	**100**	100	**100**	**100**	**100**	100	100	100	**100**	100	99.7	100	100
	CPR$_{NL4-3}$	**100**	99.1	**100**	**100**	**100**	100	100	100	**100**	100	100	100	100
	CPR$_{YU2}$	**100**	0	**100**	**100**	**100**	0	0	0	**100**	100	98.6	100	100
TenSQR	PredProp	**1**	1.6	**1**	1	1.4	**1**	**1**	**1**	**1**	1.6	2.2	1.2	0.8
	CPR$_{HXB2}$	**100**	98.9	**100**	100	99.2	**100**	**100**	**100**	**100**	92.8	96.0	99.0	0
	CPR$_{89.6}$	**100**	100	**100**	100	98.0	**100**	**100**	**100**	**100**	94.0	97.2	100	95.7
	CPR$_{JR-SCF}$	**100**	100	**100**	100	100	**100**	**100**	**100**	**100**	100	98.3	97.7	99.8
	CPR$_{NL4-3}$	**100**	99.3	**100**	100	99.5	**100**	**100**	**100**	**100**	100	99.8	99.5	99.7
	CPR$_{YU2}$	**100**	99.3	**100**	99.7	99.7	**100**	**100**	**100**	**100**	100	94.9	100	98.6
aBayesQR	PredProp	1	1	**1**	**1**	1	**1**	1	1	**1.2**	1	0.8	0.8	1.2
	CPR$_{HXB2}$	**100**	99.4	**100**	**100**	98.5	**100**	99.9	100	**100**	99.6	98	0	95.8
	CPR$_{89.6}$	**100**	98.7	**100**	**100**	98.6	**100**	100	100	**100**	92	96.5	98.9	95.5
	CPR$_{JR-SCF}$	**100**	99.6	**100**	**100**	99	**100**	100	100	**100**	98.8	97.7	99.1	98.2
	CPR$_{NL4-3}$	**100**	100	**100**	**100**	98.9	**100**	100	99.8	**100**	100	96.3	98.8	100
	CPR$_{YU2}$	**100**	99.7	**100**	**100**	99.2	**100**	99.5	99.7	**100**	100	0	98.6	99.2

3.1 Performance comparison on biallelic Solanum Tuberosum semi-experimental data

We first evaluate performance of GAEseq on realistic simulations which, for convenience and to distinguish from perhaps more rich synthetic and experimental data discussed in supplementary documents, we refer to as "semi-experimental data". The semi-experimental data is obtained by simulating mutations, shotgun sequencing procedure, read alignment and SNP calling steps in a fictitious experiment on a single individual *Solanum Tuberosum* (polyploid with $k = 4$). Details on how exactly the semi-experimental data is generated and processed can be found in Supplementary Document C. We compare the performance of GAEseq on this data with publicly available software HapCompass (Aguiar 2012), an algorithm that relies on graph-theoretic models to perform haplotype assembly, H-PoP (Xie 2016), a dynamic programming method, and AltHap (Hashemi 2018), a method based on tensor factorization. The performance of different methods is evaluated in terms of the MEC score and CPR. All the considered softwares were executed with their default settings, i.e. we follow instructions in the papers they were originally proposed; there are no parameter tuning steps required for these methods. We report the MEC scores and CPR achieved by the considered algorithms in Table 1. For each sequencing coverage, the mean and standard deviation (SD) of the adopted metrics are evaluated over 10 samples. As shown in the table, GAEseq achieves the lowest average MEC score as well as the lowest standard deviation of the MEC score at all sequencing coverage settings. Moreover, GAEseq achieves the highest average CPR at all coverage settings. Note that the MEC score increases with sequencing coverage since higher coverage implies more reads. The results demonstrate that the adopted graph abstraction enables GAEseq to achieve high accuracy of the reconstruction task by learning posterior probabilities of the origins of reads. Fig. 3 shows the precision-recall curves for data with coverage $15\times$, $25\times$ and $35\times$. Note that GAEseq performs very accuratly at high sequencing coverage while its performance deteriorates at low coverage. An extended version of Table 1 with additional coverage settings is in Supplementary Document C.

We further test the performance of GAEseq on simulated biallelic diploid, polyallelic triploid and tetraploid data, and on real Solanum Tuberosum data; in addition to H-Pop, AltHap and HapCompass, comparisons on diploid data also include performance of HapCUT2 (Edge 2017). GAEseq outperforms all the considered algorithms by achieving lower MEC score and higher CPR. Further details can be found in Supplementary Document D and E.

3.2 Performance comparison on gene-wise reconstruction of real HIV-1 data

The real HIV-1 data with pairwise distances between $2.61\%-8.45\%$ and relative frequencies between 10% and 30% is an *in vitro* viral population of 5 known HIV-1 strains generated by Illumina's MiSeq Benchtop Sequencer (Di 2014). These reads are then aligned to the HIV-1_{HXB2} reference genome. According to (Di 2014), we remove reads of length lower than 150bp and mapping quality scores lower than 60 for better results. We compare the performance of GAEseq on gene-wise reconstruction of the HIV population to that of other state-of-the-art methods such as PredictHaplo (Prabhakaran 2014), TenSQR (Ahn 2018) and aBayesQR (Ahn 2017), following their default settings. For fair benchmarking, we use the same dataset as (Ahn 2018) which is why the results of our benchmarking tests match those in (Ahn 2018). The correct phasing rate and the inferred strain frequencies are evaluated for all reconstructed strains because the ground truth for the 5 HIV-1 strains is available at (https://bmda.dmi.unibas.ch/software.html). Following (Ahn 2018), we evaluate predicted proportion by setting the parameter η needed to detect the number of HIV-1 strains to 0.09. The results in Table 2 show that GAEseq perfectly reconstructs all 5 HIV-1 strains in 8 genes while other methods correctly reconstruct components in 5 or 6 genes. This demonstrates that GAEseq's inference of read origins based on posterior probabilities enables high accuracy of the reconstruction tasks. Regarding the 5 genes where GAEseq and other methods do not achieve perfect reconstruction (p24, vpu, gp120, gp41, nef): closer examination of viral strains reconstructed by various methods suggests translocations of short viral segments within those 5 genes in the "gold standard" dataset created by (Di 2014). Those short translocation cause mismatch between the actual ground truth and the sequences (Di 2014) generated. Further results on reconstruction of HIV viral communities can be found in Supplement Document F.

4 Conclusions

In this article, we introduce auto-encoders to the problem of reconstructing components of a genomic mixture from high-throughput sequencing data that is encountered in haplotype assembly and analysis of viral communities. In particular, a graph auto-encoder is trained to group together reads that originate from the same component of a genomic mixture and impute missing information in the SNP fragment matrix by learning from the available data. The graph convolutional encoder attempts to discover origin of the reads while the decoder aims to reconstruct haplotypes and impute missing information, effectively correcting sequencing errors. Studies on semi-experimental data show that GAEseq can achieve significantly lower MEC scores and higher CPR than the competing methods. Benchmarking tests on simulated and experimental data demonstrate that GAEseq maintains good performance even at low sequencing coverage. Studies on real HIV-1 data illustrate that GAEseq outperforms existing state-of-the-art methods in viral quasispecies reconstruction.

References

Schwartz, R. 2010. Theory and algorithms for the haplotype assembly problem. *Communications in Info. & Sys.* vol. 10, no. 1, 2010, 23–38.

Clark, A. G. 2004. The role of haplotypes in candidate gene studies. *Genet Epidemiol.* vol. 27, no. 4, 2004, 321–33.

Sabeti, P.; Reich, D.; Higgins, J.; Levine, H.; and Richter, D. 2002. Detecting recent positive selection in the human genome from haplotype structure. *Nature*, 419(6909):832–37, 2002.

Lancia, G.; Bafna, V.; Istrail, S.; Lippert, R.; and Schwartz, R. 2001. SNPs problems, complexity, and algorithms. *European symposium on algorithms*, vol. 1, Springer: 2001.182–93.

Duitama, J.; Huebsch, T.; McEwen, G.; Suk, E.; and Hoehe, MR. 2010. Refhap: a reliable and fast algorithm for single individual haplotyping. *Proceedings of the First ACM International Conference on Bioinformatics and Computational Biology*, ACM: 2010. 160–169.

Lippert, R.; Schwartz, R.; Lancia, G.; and Istrail, S. 2002 Algorithmic strategies for the single nucleotide polymorphism haplotype assembly problem. *Brief Bioinformatics*, 2002, 3(1):23–31.

Xie, M.; Wu, Q.; Wang, J.; and Jiang, T. 2016. H-PoP and H-PoPG: Heuristic partitioning algorithms for single individual haplotyping of polyploids. *Bioinformatics*, 2016, 32(24):3735–44.

Pirola, Y.; Zaccaria, S.; Dondi, R.; Klau, G.; Pisanti, N.; and Bonizzoni, P. 2015. Hapcol: accurate and memory-efficient haplotype assembly from long reads. *Bioinformatics*, 2015, 32(11), 1610–1617.

Kuleshov, V. 2014. Probabilistic single-individual haplotyping. *Bioinformatics*, 2014, 30(17):379–85.

Patterson, M.; Marschall, T.; Pisanti, N.; Van, Iersel L.; and Stougie, L. 2015. Whatshap: weighted haplotype assembly for future-generation sequencing reads. *J Comput Biol.*, 2015, 22(6):498–509.

Bonizzoni, P.; Dondi, R.; Klau, G.; Pirola, Y.; Pisanti, N.; and Zaccaria, S. 2016. On the minimum error correction problem for haplotype assembly in diploid and polyploid genomes. *J Comput Biol.*, 2016, 23(9):718–36.

Edge, P.; Bafna, V.; and Bansal, V. 2017. Hapcut2: robust and accurate haplotype assembly for diverse sequencing technologies. *Genome Res.*, 2017; 27(5):801–12.

Aguiar, D., and Istrail, S. 2012. Hapcompass: a fast cycle basis algorithm for accurate haplotype assembly of sequence data. *J Comput Biol.* 2012; 19(6):577–90.

Duitama, J.; McEwen, G.; Huebsch, T.; Palczewski, S.; and Schulz, S. 2011. Fosmid-based whole genome haplotyping of a hapmap trio child: evaluation of single individual haplotyping techniques. *Nucleic Acids Res.*, 2011, 40(5), 2041–2053.

Das, S.; and Vikalo, H. 2015. SDhaP: haplotype assembly for diploids and polyploids via semi-definite programming. *BMC Genomics*, 2015; 16(1):260.

Puljiz, Z.; and Vikalo, H. 2016. Decoding genetic variations: communications-inspired haplotype assembly. *IEEE/ACM Trans Comput Biol Bioinform (TCBB)*, 2016; 13(3):518–30.

Berger, E.; Yorukoglu, D.; Peng, J.; and Berger, B. 2014. Haptree: A novel Bayesian framework for single individual polyplotyping using NGS data. *PLoS Comput Biol.* 2014; 10(3):e1003502.

Ahn, S.; Ke, Z.; and Vikalo, H. (2018). Viral quasispecies reconstruction via tensor factorization with successive read removal. *Bioinformatics (Oxford, England)*, 34(13), i23–i31.

Wang, R.; Wu, L.; Li, Z.; and Zhang, X. 2005. Haplotype reconstruction from SNP fragments by minimum error correction. *Bioinformatics*, 2005, 21(10):2456–2462.

Chen, Z.; Deng, F.; and Wang, L. 2013. Exact algorithms for haplotype assembly from whole-genome sequence data. *Bioinformatics*, 2013, 29(16):1938–1945.

Levy, S.; Sutton, G.; Ng, P.; Feuk, L.; and Halpern, A. 2007 The diploid genome sequence of an individual human. *PLoS Biol.*, 2007, 5(10):254.

Bansal, V.; Halpern, A.; Axelrod, N.; and Bafna, V. 2008. An MCMC algorithm for haplotype assembly from whole-genome sequence data. *Genome Res.*, 2008; 18(8):1336–46.

Kim, J.; Waterman M.; and Li, L. 2007. Diploid genome reconstruction of ciona intestinalis and comparative analysis with ciona savignyi. *Genome Res.* 2007; 17(7):1101–10.

Goodfellow I.; Bengio, Y.; and Courville A. 2016. Deep Learning. *MIT Press*.

Lippert, R.; Schwartz, R.; Lancia, G.; and Istrail, S. 2002. Algorithmic strategies for the single nucleotide polymorphism haplotype assembly problem. *Briefings in bioinformatics*, 3(1), 23–31.

Motazedi, E.; Finkers, R.; Maliepaard, C.; and de Ridder, D. 2018. Exploiting next-generation sequencing to solve the haplotyping puzzle in polyploids: a simulation study. *Briefings in bioinformatics*, 19(3), 387–403.

Cai, C.; Sanghavi, S.; and Vikalo, H. 2016. Structured low-rank matrix factorization for haplotype assembly. *IEEE J Sel Top Sign Proc.* 2016; 10(4):647–57.

Hashemi, A.; Zhu, B.; and Vikalo, H. 2018. Sparse tensor decomposition for haplotype assembly of diploids and polyploids. *BMC Genomics*, 2018; 19(4), 191.

Rianne van den Berg, Thomas N. Kipf and Max Welling 2017. Graph Convolutional Matrix Completion. *arXiv:1706.02263*.

Kipf, Thomas N. and Max Welling 2016. Variational Graph Auto-Encoders. *CoRR*, abs/1611.07308.

Di, F.; Töpfer, A.; Rey, M.; Prabhakaran, S.; Duport, Y.; Leemann, C.; Schmutz, S.; Campbell, N. K.; Joos, B.; and Lecca, M. R. 2014. Full-length haplotype reconstruction to infer the structure of heterogeneous virus populations. *Nucleic acids research*, 42(14), e115.

Ahn, S.; and Vikalo, H. 2017. aBayesQR: A bayesian method for reconstruction of viral populations characterized by low diversity. In *International Conference on Research in Computational Molecular Biology*, pages 353–369. Springer.

Zagordi, O.; Bhattacharya, A.; Eriksson, N.; and Beerenwinkel, N. 2011. Shorah: estimating the genetic diversity of a mixed sample from next-generation sequencing data. *BMC bioinformatics*, 12(1), 119.

Astrovskaya, I.; Tork, B.; Mangul, S.; Westbrooks, K.; Măndoiu, I.; Balfe, P.; Zelikovsky, A. 2011. Inferring viral quasispecies spectra from 454 pyrosequencing reads. *BMC bioinformatics*, 12(6), 1.

Prosperi, M. C; and Salemi, M. 2012. Qure: software for viral quasispecies reconstruction from next-generation sequencing data. *Bioinformatics*, 28(1), 132–133.

Prabhakaran, S.; Rey, M.; Zagordi, O.; Beerenwinkel, N.; and Roth, V. 2014. Hiv haplotype inference using a propagating dirichlet process mixture model. *IEEE/ACM Trans. on Comput. Biol. Bioinform. (TCBB)*, 11(1), 182–191.

Töpfer, A.; Zagordi, O.; Prabhakaran, S.; Roth, V.; Halperin, E.; and Beerenwinkel, N. 2013. Probabilistic inference of viral quasispecies subject to recombination. *Journal of Computational Biology*, 20(2), 113–123.

Socher, R.; Pennington, J.; Huang, Eric H.; Ng, Andrew Y.; and Manning, Christopher D. 2011. Semi-supervised Recursive Autoencoders for Predicting Sentiment Distributions. *Conference on Empirical Methods in Natural Language Processing*, EMNLP(11), 151-161.

Fukushima K. C. 1975. a self-organizing multilayered neural network. *Biol Cybern*, 20(3-4), 121-36.

Masci J.; Meier U.; and Ciresan D. 2011. Stacked convolutional auto-encoders for hierarchical feature extraction. *Artificial Neural Networks and Machine Learning ICANN*, 529.

Supplementary Document A : Computational settings

The models were implemented on a 3.70GHz Intel i7-8700K processor, 2 NVIDIA GeForce GTX 1080Ti computer graphics cards and 32GB RAM. Randomness of the initial weights of the auto-encoder may cause the neural network to remain in a local minimum during training. To overcome this, we run GAEseq multiple times and choose the result with the lowest MEC score. Given a SNP fragment matrix, we run GAEseq 200 times, train 200 models and get 200 reconstructed haplotype matrix candidates; the algorithm selects the candidate corresponding to the lowest MEC score automatically. In the GAEseq software, users can specify how many times to run the algorithm; the software will run automatically as opposed to manually running GAEseq multiple times.

As for hyperparameters, the number of graph convolutional layers in the auto-encoder was set to 2 (in particular, one read-nodes-to-SNP-nodes layer and one SNP-nodes-to-read-nodes layer); dimension of messages reduces linearly during message passing between the layers. For example, if the number of reads is m, the haplotype length is n, the ploidy is k and we use 2 graph convolutional layers and a dense layer, the dimensions of the weight and bias matrix of the first and second layer are $n \times \lceil (n - \frac{n-k}{3}) \rceil$ and $\lceil (n - \frac{n-k}{3}) \rceil \times \lceil (n - 2 \times \frac{n-k}{3}) \rceil$, respectively. The dimensions of the weight and bias matrix of the denser layer are set to $\lceil (n - 2 \times \frac{n-k}{3}) \rceil \times k$ and $m \times k$, respectively. We use the Adam optimizer (Diederik 2015), set the step size to 0.0001, and set all other parameters to their default values in Tensorflow. We also use Xavier initialization (Xavier 2010) with default settings and the number of epoches set to 100. In our studies, we found that an architecture with two graph convolutional layers achieves significantly better results than state-of-the-art haplotype assembly methods. To ensure the model generalizes well to unobserved entries, we added dropout regularization to message passing between the layers; for each layer, the dropout probability is 0.1. For all experiments on viral quasispecies reconstruction, the initial number of clusters k_0 is set to 2.

Supplementary Document B : Determining the number of components in a viral quasispecies

When reconstructing haplotypes sampled by a collection of sequencing reads, GAEseq requires as input the number of haplotypes, k. While the ploidy of an individual organism in the haplotype assembly problem is known a priori, cardinality of a viral community needs to be estimated. To determine k, we examine the improvement rate of the MEC score defined as

$$\text{MECimpr}(k) = \frac{\text{MEC}(k) - \text{MEC}(k+1)}{\text{MEC}(k)}. \qquad (1)$$

Recall that the MEC score is defined as the smallest number of the observed entries in R that need to be altered such that the resulting data is consistent with having originated from k distinct haplotypes. The score decreases monotonically with k; however, once k reaches the actual number of components, the improvement rate of the MEC score (MECimpr) saturates. To find the saturation point, we compare MECimpr with a pre-defined threshold. Following (Ahn 2018), the number of components is determined via binary search. Specifically, starting from an initial k_0, the number of components is updated as $k_\tau \leftarrow 2k_{\tau-1}$ until MECimpr$(k_\tau) \leq \eta$; at this point, the number of components starts to decrease as $k_{\tau+1} \leftarrow \lfloor (k_\tau + \max\{1, k_i\})/2 \rfloor$ where $\{i \in \{1, \cdots, \tau-1\} : k_i \leq k_\tau\}$. Once MECimpr$(k_\tau) > \eta$, the number of components increases again as $k_{\tau+1} \leftarrow \lfloor (k_\tau + \min k_i)/2 \rfloor$ where $\{i \in \{1, \cdots, \tau-1\} : k_i > k_\tau\}$. If $k_\tau = k_{\tau-1}$, the search procedure stops by assigning $k_{\tau+1} \leftarrow k_\tau + 1$ which is the estimated number of strains. The recommended choice of the threshold η is discussed in (Ahn 2017) where the estimation of the number of components via MECimpr was demonstrated to be robust with respect to the choice of the threshold.

Supplementary Document C : Performance comparison on biallelic Solanum Tuberosum semi-experimental data

The semi-experimental data is obtained by simulating mutations, shotgun sequencing procedure, read alignment and SNP calling steps in an experiment on a single individual *Solanum Tuberosum*. In particular, we use *Haplogenerator* (Motazedi 2018) to generate haplotypes by introducing independent mutations that follow the lognormal distribution of a randomly selected genome region from *Solanum Tuberosum* chromosome 5 (Potato Genome Sequencing Consortium 2011) of length 5000 bp. The mean distance between neighboring SNPs and the standard deviation (SD) are set to 21 bp and 27 bp, respectively, as previously suggested by (Motazedi 2018). Due to *Haplogenerator*'s limitations, we constrain mutations to transitions and do not consider transversions (i.e., mutations are constrained to be between A and C and between G and T). 2×250 bp-long Illumina's MiSeq reads of inner distance 50 bp and standard deviation 10 bp are generated to uniformly sample haplotypes using *ART* software (Huang 2012) with default setting. Following this step, the generated reads are aligned to the reference genome using the BWA-MEM algorithm (Li 2009); the reads having mapping quality score lower than 60 or being shorter than 70 bp are discarded. SNPs are called if, at any given site, the abundance of a minor allele exceeds a predetermined threshold; the SNP fragment matrix is formed by collecting all such heterozygous sites. Seven different sets of semi-experimental data obtained by sampling at varying coverage ($10\times$, $15\times$, $20\times$, $25\times$, $30\times$, $35\times$ and $40\times$) are generated; each set consists of 10 samples. We first generate genome regions of length 5000 bp by partitioning the *Solanum Tuberosum* chromosome 5 and then randomly select 70 among them (generated haplotypes and reads are different for each sample). The sequencing error rate is automatically set by the built-in quality profiles of *ART* inferred from large amounts of recalibrated sequencing data (Huang 2012). Table 1 shows the performance comparison of GAEseq, AltHap, HapCompass and H-PoP on biallelic Solanum Tuberosum semi-experimental data.

Table 1: Performance comparison of GAEseq, AltHap, HapCompass and H-PoP on biallelic Solanum Tuberosum semi-experimental data.

Coverage		MEC Mean	SD	CPR Mean	SD
10	GAEseq	**18.500**	**4.552**	**0.848**	0.074
	HapCompass	100.300	43.584	0.769	**0.039**
	H-PoP	19.700	25.254	0.803	0.086
	AltHap	64.100	32.953	0.727	0.072
15	GAEseq	**8.200**	**4.686**	**0.822**	0.048
	HapCompass	100.700	66.150	0.763	**0.046**
	H-PoP	28.700	32.667	0.783	0.066
	AltHap	59.100	28.125	0.709	0.054
20	GAEseq	**16.800**	**15.873**	**0.862**	0.062
	HapCompass	95.600	53.883	0.795	**0.047**
	H-PoP	30.500	37.023	0.791	0.078
	AltHap	82.100	56.658	0.737	0.068
25	GAEseq	**8.400**	**4.719**	**0.831**	0.081
	HapCompass	124.800	132.156	0.810	0.063
	H-PoP	33.800	47.434	0.798	**0.046**
	AltHap	92.600	83.649	0.756	0.068
30	GAEseq	**27.200**	**19.887**	**0.914**	**0.033**
	HapCompass	306.800	187.934	0.796	0.081
	H-PoP	34.200	32.798	0.879	0.088
	AltHap	263.000	499.659	0.762	0.133
35	GAEseq	**10.700**	**3.234**	**0.857**	0.087
	HapCompass	217.400	174.135	0.775	**0.072**
	H-PoP	41.700	53.971	0.823	0.094
	AltHap	164.000	101.583	0.754	0.093
40	GAEseq	**16.400**	**7.333**	**0.835**	**0.034**
	HapCompass	208.000	176.699	0.833	0.070
	H-PoP	30.4	28.487	0.823	0.102
	AltHap	195.8	281.641	0.762	0.084

Supplementary Document D : Performance comparison on simulated biallelic diploid data and polyallelic triploid and tetraploid data.

To further test GAEseq, we evaluate its performance on synthetic data. Once again we use *Haplogenerator* (Motazedi 2018) to generate haplotypes of a randomly synthesized reference genome of length 5000 bp. The mean distance between neighboring SNPs and the standard deviation (SD) are set to 5 bp and 3 bp respectively, creating haplotype blocks of length about 500. All the possible mutations were allowed and set to be equally likely, leading to not only biallelic but also polyallelic SNPs in the synthesized haplotype data. Illumina's MiSeq read generation, read alignment and SNP calling procedures are implemented following the same procedure as in the case of semi-experimental data from Section 3.1. The data synthesized in this fashion consists of 24 different sets, each with 10 samples, as we explore different ploidy (k = 2, 3 and 4) and sequencing coverage (5×, 10×, 15×, 20×, 25×, 30×, 35× and 40×).

For the diploid synthetic data sets, we represent an allele by 0 if it coincides with the corresponding reference allele and by 1 if it is an alternative allele. SNP positions with only alternative alleles are removed. In addition to H-PoP, HapCompass and AltHap, we also compare GAEseq with HapCUT2 (Edge 2017); by design, use of HapCUT2 is limited to haplotype assembly of diploids. The metrics of performance are the previously introduced MEC score and CPR. Table 2 shows the mean and standard deviation of the MEC score and CPR for diploid data. The results are evaluated over 10 samples for each combination of ploidy and coverage. GAEseq achieves the lowest average MEC score and the lowest standard deviation of the MEC score for almost all coverage settings; its performance is followed by those of H-PoP, HapCompass, HapCut2 and AltHap. The average CPR achieved by GAEseq is very close to 1 for all coverage settings, indicating that GAEseq is able to near-perfectly reconstruct haplotypes of diploid species even when the coverage is very low; its performance is followed by those of H-PoP, HapCut2, HapCompass and AltHap. When the coverage is 20×, the average CPR achieved by GAEseq is 100% while it is approximately 98.9%, 97.2%, 96.1% and 74.3% for H-PoP, HapCut2, HapCompass and AltHap, respectively.

For the polyploid synthetic data sets, both H-PoP and HapCompass are restricted to reconstruction of biallelic haplotypes and are not applicable to the assembly of polyallelic ones. Furthermore, recall that HapCUT2 can only be ap-

Table 2: Performance comparison of GAEseq, HapCut2, HapCompass, H-PoP and AltHap on simulated biallelic diploid data.

		MEC		CPR	
Coverage		Mean	SD	Mean	SD
5	GAEseq	**23.300**	**4.165**	**0.996**	**0.002**
	HapCUT2	110.500	23.922	0.975	0.006
	HapCompass	87.500	25.903	0.965	0.010
	H-Pop	40.000	30.551	0.989	0.011
	AltHap	884.200	659.565	0.699	0.204
10	GAEseq	**30.700**	**6.667**	**0.999**	**0.001**
	HapCUT2	213.600	63.132	0.980	0.005
	HapCompass	159.600	58.329	0.974	0.005
	H-Pop	34.600	6.736	0.997	0.004
	AltHap	583.900	948.344	0.796	0.218
15	GAEseq	**47.800**	**8.587**	**0.999**	**0.001**
	HapCUT2	339.800	59.066	0.978	0.003
	HapCompass	268.300	67.003	0.971	0.005
	H-Pop	47.900	9.539	0.998	0.002
	AltHap	342.900	379.213	0.852	0.169
20	GAEseq	**70.900**	**10.754**	**1.000**	**0.001**
	HapCUT2	519.400	57.386	0.972	0.010
	HapCompass	408.000	81.067	0.961	0.018
	H-Pop	129.700	191.788	0.989	0.030
	AltHap	668.400	579.261	0.787	0.201
25	GAEseq	**85.200**	**16.130**	**1.000**	**0.001**
	HapCUT2	613.000	157.786	0.977	0.006
	HapCompass	460.700	97.637	0.968	0.007
	H-Pop	85.700	17.192	0.998	0.003
	AltHap	1151.600	649.058	0.743	0.150
30	GAEseq	**97.800**	8.954	**1.000**	**0.000**
	HapCUT2	685.300	180.714	0.979	0.006
	HapCompass	591.600	150.400	0.968	0.009
	H-Pop	98.000	**8.743**	0.999	0.001
	AltHap	554.000	612.292	0.871	0.185
35	GAEseq	**107.300**	8.138	**1.000**	**0.001**
	HapCUT2	827.600	202.643	0.978	0.006
	H-Pop	702.200	180.647	0.968	0.007
	H-Pop	107.900	**8.006**	0.999	0.001
	AltHap	668.800	730.814	0.891	0.146
40	GAEseq	**124.000**	10.499	**1.000**	**0.001**
	HapCUT2	1015.400	219.442	0.977	0.006
	HapCompass	896.500	204.603	0.965	0.008
	H-Pop	124.500	**10.277**	0.999	**0.001**
	AltHap	1073.300	1099.181	0.847	0.184

plied to diploid haplotypes. We therefore limit performance comparison of GAEseq on polyploid synthetic data to only AltHap; Tables 3 and 4 illustrate the mean and standard deviation of the MEC score and CPR for triploid and tetraploid data, respectively. The results are evaluated over 10 samples for each combination of ploidy and coverage. As can be seen in these tables, GAEseq outperforms AltHap for all ploidy and coverage settings. As shown in Table 3, GAEseq performs well on triploid data, achieving 92% average CPR and relatively small standard deviation even for the low coverage of $5\times$; at the same time, performance of AltHap deteriorates rapidly with increased ploidy, achieving 72% average CPR while GAEseq achieves 98.2% at coverage $30\times$. As illustrated in Table 4, in applications to tetraploid data the performance of GAEseq starts to gracefully deteriorate – when the coverage is $10\times$, GAEseq achieves average CPR of approximately 80% while in the same scenario AltHap achieves average CPR of approximately 65%. When the coverage is increased to $40\times$, GAEseq achieves average CPR of approximately 87.8% while AltHap achieves average CPR of approximately 76.2%.

Table 3: Performance comparison of GAEseq and AltHap on simulated polyallelic triploid data.

		MEC		CPR	
Coverage		Mean	SD	Mean	SD
5	GAEseq	**103.400**	**51.379**	**0.920**	**0.047**
	AltHap	1908.500	237.324	0.559	0.059
10	GAEseq	**112.800**	**45.917**	**0.958**	**0.037**
	AltHap	1769.300	948.754	0.760	0.091
15	GAEseq	**165.800**	**106.999**	**0.945**	**0.073**
	AltHap	1058.100	864.563	0.796	0.123
20	GAEseq	**241.300**	**159.657**	**0.959**	**0.047**
	AltHap	1287.100	578.507	0.682	0.070
25	GAEseq	**314.900**	**158.326**	**0.934**	**0.070**
	AltHap	1430.200	757.482	0.775	0.093
30	GAEseq	**292.400**	**203.242**	**0.974**	**0.040**
	AltHap	2133.200	1082.576	0.729	0.109
35	GAEseq	**306.200**	**196.918**	**0.982**	**0.037**
	AltHap	2928.700	869.617	0.723	0.075
40	GAEseq	**502.200**	**247.380**	**0.922**	**0.088**
	AltHap	2943.600	1113.480	0.737	0.104

Table 4: Performance comparison of GAEseq and AltHap on simulated polyallelic tetraploid data.

		MEC		CPR	
Coverage		Mean	SD	Mean	SD
5	GAEseq	**266.700**	**46.371**	**0.739**	**0.041**
	AltHap	2641.700	410.159	0.544	0.056
10	GAEseq	**415.100**	**74.608**	**0.800**	**0.051**
	AltHap	2807.200	938.668	0.658	0.075
15	GAEseq	**592.200**	**112.282**	**0.798**	**0.054**
	AltHap	2742.500	1055.672	0.718	0.081
20	GAEseq	**628.900**	**245.841**	**0.843**	**0.047**
	AltHap	1929.700	1008.766	0.729	0.063
25	GAEseq	**881.900**	**189.987**	**0.845**	**0.058**
	AltHap	1987.100	1091.893	0.779	0.084
30	GAEseq	**944.100**	**182.440**	**0.848**	**0.041**
	AltHap	2265.200	1277.366	0.759	0.051
35	GAEseq	**815.900**	**295.195**	**0.866**	**0.063**
	AltHap	3906.400	1131.654	0.747	0.056
40	GAEseq	**949.500**	**319.238**	**0.878**	**0.046**
	AltHap	3775.300	1036.702	0.762	0.075

Supplementary Document E : Performance comparison on real Solanum Tuberosum data

We further test the performance of GAEseq on real potato data (accession SRR6173308) at *Solanum Tuberosum* chromosome 5 (Potato Genome Sequencing Consortium 2011). The 10 samples of real potato data are generated by first randomly selecting 10 genome regions of length varying from 5032 to 7573 and then aligning the Illumina HiSeq 2000 paired-end reads to the selected genome regions. After the read alignment step using the BWA-MEM algorithm (Li 2009), the SNP calling step is implemented to create the SNP fragment matrix. Reads having mapping quality score lower than 60 or shorter than 70 bp are discarded. Since the ground truth haplotypes are not available for this dataset, we only evaluate the performance of GAEseq and the competing methods in terms of the MEC score. Table 5 compares the performance of GAEseq, AltHap, HapCompass and H-PoP averaged over 10 selected regions of the real Solanum Tuberosum data. As can be seen from the table, GAEseq outperforms all the competing schemes in terms of both the average MEC score and its standard deviation, achieving 379.8 average MEC score. GAEseq is followed by H-PoP and AltHap while HapCompass achieves the highest average MEC score.

Table 5: Performance comparison of GAEseq, AltHap, HapCompss and H-PoP on the real Solanum Tuberosum data.

	MEC	
	Mean	SD
GAEseq	**379.8**	**271.61**
HapCompass	2726	2393.7
H-PoP	409.5	282.24
AltHap	742.1	469.5

Supplementary Document F : Further results on reconstruction of HIV viral communities

Table 6 shows the gene-wise reconstruction results on the real HIV-1 data that include inferred frequencies (omitted from Table 2 in the main paper for brevity).

We further evaluate the performance of GAEseq on the 4036bp long gag-pol region. Following (Ahn 2018), we divide the gag-pol region into overlapping blocks, reconstruct the viral components in each block independently, and combine the results to reconstruct the full region of interest. Specifically, the region is divided into a sequence of blocks of length 500bp where the consecutive blocks overlap by 250bp. We run GAEseq to perform reconstruction of viral components in each of the total 18 blocks and merge the results to retrieve the entire region of interest. Particularly, the mismatches between strains reconstructed on two consecutive blocks in the overlapping region are corrected based on majority voting using reads that are covering the mismatched positions and are assigned to the aligned strains. Following this procedure, GAEseq perfectly reconstructed all of 5 HIV-1 strains in the gag-pol region, achieving 100% Reconstruction Rate for all 5 strains and Predicted Proportion of 1 on 355241 remained paired-end reads. The frequencies of 5 HIV-1 strains are estimated as $15.21\%, 19.34\%, 25.56\%, 27.61\%$ and 12.27% by counting the proportion of reads assigned to the same strain; these results are consistent with the frequencies estimated by aBayesQR and TenSQR softwares.

Table 6: Performance comparisons of GAEseq, TenSQR, aBayesQR and PredictHap on a real HIV-1 5-virus-mix data.

		p17	p24	p2-p6	PR	RT	RNase	int	vif	vpr	vpu	gp120	gp41	nef
GAEseq	PredProp	**1**	1	**1**	**1**	**1.2**	**1**	**1**	**1**	**1**	1.2	1	1	1
	CPR$_{HXB2}$	**100(20.5)**	99.4(17.1)	**100(21)**	**100(30.9)**	**100(12.1)**	**100(9.6)**	**100(13.6)**	**100(10.4)**	**100(6.6)**	100(34.3)	96.2(8.7)	96.7(2.8)	100(6.6)
	CPR$_{89.6}$	**100(18.8)**	99.4(21.8)	**100(20)**	**100(18)**	**100(18.2)**	**100(20.9)**	**100(18.2)**	**100(20.4)**	**100(20.3)**	99.2(10.5)	99.4(24.1)	100(25.6)	98.2(22.9)
	CPR$_{JR-SCF}$	**100(30.9)**	100(31.5)	**100(27)**	**100(21.6)**	**100(23.5)**	**100(20.2)**	**100(21.5)**	**100(29.8)**	**100(34.6)**	100(36.4)	99.9(33.0)	100(27)	99.3(19.7)
	CPR$_{NL4-3}$	**100(17.4)**	100(18.3)	**100(14.1)**	**100(19.7)**	**100(30.6)**	**100(33.1)**	**100(37.1)**	**100(32.8)**	**100(30.6)**	100(7.9)	100(29.6)	100(34.5)	99.8(39.1)
	CPR$_{YU2}$	**100(12.3)**	100(11.2)	**100(18)**	**100(9.9)**	**100(11.9)**	**100(16.2)**	**100(9.6)**	**100(6.6)**	**100(7.9)**	100(10.2)	99.6(4.6)	100(10)	98.1(11.7)
PredictHap	PredProp	**1**	0.6	**1**	**1**	**1**	0.8	0.8	0.8	**1**	0.8	0.8	0.8	0.8
	CPR$_{HXB2}$	**100(17.8)**	0(0)	**100(18.7)**	**100(15.2)**	**100(12.2)**	98.9(25.4)	100(12.1)	100(17.7)	**100(10.2)**	93.2(10.8)	0(0)	0(0)	0(0)
	CPR$_{89.6}$	**100(19.9)**	100(46.4)	**100(21.7)**	**100(22.2)**	**100(19.4)**	100(18.2)	99.8(27.6)	100(20.9)	**100(22.1)**	0(0)	97.8(20.7)	100(26.7)	98.8(20.7)
	CPR$_{JR-SCF}$	**100(31.9)**	100(21.8)	**100(30.3)**	**100(26.9)**	**100(23.4)**	100(23.2)	100(22.3)	100(24.9)	**100(23.7)**	100(34.1)	99.7(42.7)	100(28.9)	100(23.2)
	CPR$_{NL4-3}$	**100(17)**	99.1(31.8)	**100(16.4)**	**100(20.9)**	**100(30.2)**	100(33.2)	100(38.1)	100(36.6)	**100(35.5)**	100(47.1)	100(28.6)	100(32.7)	100(39.3)
	CPR$_{YU2}$	**100(13.4)**	0(0)	**100(12.9)**	**100(14.8)**	**100(14.7)**	0(0)	0(0)	0(0)	**100(8.5)**	100(7.9)	98.6(7.9)	100(11.7)	100(16.9)
TenSQR	PredProp	**1**	1.6	**1**	1	1.4	**1**	**1**	**1**	**1**	1.6	2.2	1.2	0.8
	CPR$_{HXB2}$	**100(18.7)**	98.9(13.1)	**100()17.4**	100(9.9)	99.2(12.1)	**100(9.2)**	**100(8.1)**	**100(9.6)**	**100(7.2)**	92.8(5.9)	96.0(18)	99.0(11.5)	0(0)
	CPR$_{89.6}$	**100(18.4)**	100(19.6)	**100(20.1)**	100(17.2)	98.0(13.5)	**100(17.2)**	**100(16.7)**	**100(25)**	**100(19.3)**	94.0(15)	97.2(10.3)	100(27.8)	95.7(26)
	CPR$_{JR-SCF}$	**100(33.8)**	100(33)	**100(33.6)**	100(21.7)	100(20.7)	**100(24.6)**	**100(23.3)**	**100(20.5)**	**100(20.3)**	100(31.4)	98.3(33.5)	97.7(18.8)	99.8(19)
	CPR$_{NL4-3}$	**100(17)**	99.3(19.7)	**100(17.2)**	100(21.4)	99.5(26.7)	**100(37.7)**	**100(41.2)**	**100(38.4)**	**100(46.2)**	100(38.8)	99.8(9.2)	99.5(23.2)	99.7(42.7)
	CPR$_{YU2}$	**100(12.1)**	99.3(14.6)	**100(7.7)**	99.7(29.8)	99.7(14.5)	**100(11.4)**	**100(10.7)**	**100(6.5)**	**100(7.1)**	100(4.1)	94.9(10.5)	100(10.2)	98.6(12.3)
aBayesQR	PredProp	1	1	**1**	**1**	1	**1**	1	1	**1.2**	1	0.8	0.8	1.2
	CPR$_{HXB2}$	**100(16.3)**	99.4(21.1)	**100(22.2)**	**100(12.5)**	98.5(24.3)	**100(16.1)**	99.9(9.7)	100(9.2)	**100(16.4)**	99.6(17)	98(30.3)	0(0)	95.8(11.4)
	CPR$_{89.6}$	**100(27.1)**	98.7(17)	**100(17.3)**	**100(17.3)**	98.6(18.1)	**100(19.7)**	100(22.2)	100(20.6)	**100(16.3)**	92(10.4)	96.5(20.2)	98.9(23.7)	95.5(16.4)
	CPR$_{JR-SCF}$	**100(31.3)**	99.6(24.6)	**100(25.8)**	**100(29.9)**	99(21.5)	**100(22.1)**	100(20.8)	100(32.7)	**100(27)**	98.8(26.7)	97.7(21.4)	99.1(29.7)	98.2(21.1)
	CPR$_{NL4-3}$	**100(12.9)**	100(21.6)	**100(25.6)**	**100(20.1)**	98.9(17.7)	**100(30)**	100(39.5)	99.8(28.5)	**100(23.2)**	100(41.3)	96.3(28)	98.8(36.6)	100(31.8)
	CPR$_{YU2}$	**100(12.4)**	99.7(15.8)	**100(9.2)**	**100(20.3)**	99.2(18.5)	**100(12.2)**	99.5(7.9)	99.7(9)	**100(17.1)**	100(4.6)	0(0)	98.6(10.1)	99.2(14)

Predicted Proportion (PredProp) and Correct Phasing Rate (CPR (%)) for GAEseq, PredictHaplo, TenSQR and aBayesQR applied to reconstruction of HIV-1HXB2, HIV-189.6, HIV-1JR-CSF, HIV-1NL4-3 and HIV-1YU2 for all 13 genes of the HIV-1 dataset. Frequencies are reported in parenthesis.

References

Diederik P. Kingma and Jimmy Ba 2015. Adam: A Method for Stochastic Optimization. *arXiv:1412.6980 [cs.LG].*

Xavier Glorot and Yoshua Bengio 2010. Understanding the difficulty of training deep feedforward neural networks. *Proceedings of the thirteenth international conference on artificial intelligence and statistics*, 249-256.

Ahn, S.; Ke, Z.; and Vikalo, H. (2018). Viral quasispecies reconstruction via tensor factorization with successive read removal. *Bioinformatics (Oxford, England)*, 34(13), i23–i31.

Ahn, S.; and Vikalo, H. 2017. aBayesQR: A bayesian method for reconstruction of viral populations characterized by low diversity. In *International Conference on Research in Computational Molecular Biology*, pages 353–369. Springer.

Motazedi, E.; Finkers, R.; Maliepaard, C.; and de Ridder, D. 2018. Exploiting next-generation sequencing to solve the haplotyping puzzle in polyploids: a simulation study. *Briefings in bioinformatics*, 19(3), 387–403.

Potato Genome Sequencing Consortium 2011. Genome sequence and analysis of the tuber crop potato. *Nature*, 475, 189–195.

Huang, W.; and Li, L.; Myers, J. R. and Marth, G. T. 2012. ART: a next-generation sequencing read simulator. *Bioinformatics*, 28(4), 593–594.

Li, H.; and Durbin, R. 2009. Fast and accurate short read alignment with burrows-wheeler transform. *Bioinformatics*, 25(14), 1754–1760.

Edge, P.; Bafna, V.; and Bansal, V. 2017. Hapcut2: robust and accurate haplotype assembly for diverse sequencing technologies. *Genome Res.*, 2017; 27(5):801–12.